SUPPLEMENTARY FILE

Galvanic Replacement Reaction and Kirkendall Effect in Room Temperature Synthesis of Tubular $NiSe_2$: A Nanozyme Catalyst with Peroxidase-Like Activity

Sougata Sarkar,[a] Yuichi Negishi,[b] Tarasankar Pal[c,*]

[a]*Department of Chemistry, Ramakrishna Mission Vivekananda Centenary College, Rahara, Kolkata - 700118, India*

[b]*Department of Applied Chemistry, Faculty of Science, Tokyo University of Science, 1–3 Kagurazaka, Shinjuku-ku, Tokyo162-8601, Japan*

[c]*Department of Chemical Sciences, University of Johannesburg, P. O. Box 524, Auckland Park 2006, Kingsway Campus, South Africa*

E-mail: tpal@chem.iitkgp.ernet.in

EXPERIMENTAL SECTION

Analytical Methods:

Field Emission Scanning Electron Microscopy (FESEM): The morphology of the samples was analyzed by field emission scanning electron microscopy (FESEM) using (Supra 40, Carl Zeiss Pvt. Ltd.) microscope. Compositional analysis of the sample was done by an energy dispersive X-ray micro-analyzer (OXFORD ISI 300 EDAX) attached to the scanning electron microscope.

Transmission Electron Microscopy (TEM): Transmission electron microscopic (TEM) analyses of the samples were carried out on a Hitachi H-9000 NAR transmission electron microscope. Samples were prepared by sonicating the powders with alcohol and then placing a drop of solution on a carbon coated copper grid followed by solvent evaporation in vacuum.

X-ray diffraction (XRD): XRD patterns of the different samples were recorded on a Philips PW-1710 X-ray diffractrometer (40 kV, 20 mA) using Cu *Kα* radiation (λ=1.5418 Å) in the

2θ range of 20°-90° at a scanning rate of 0.5° min^{-1}. The XRD data were analyzed using JCPDS software.

X-ray Photoelectron Spectroscopy (XPS): The chemical state of the element on the surface was analyzed by a VG Scientific ESCALAB MK II spectrometer (UK) equipped with a Mg KR excitation source (1253.6 eV) and a five-channeltron detection system. The samples were prepared by placing one drop of the sample suspension in ethanol onto a clean glass slide and then allowing them to dry in air.

Gas sorption measurement: Nitrogen adsorption and desorption measurements were performed at 77K using a Quantachrome Autosorb Automated Gas Sorption System utilizing Barrett-Emmett-Teller (BET) calculations for surface area and BJH calculations for pore size distribution after the samples were degassed in vacuum overnight.

UV-Visible Spectroscopy: Absorption spectrum was recorded in a Perkin Elmer (Lambda 365) spectrophotometer.

FIGURES AND FIGURE CAPTIONS

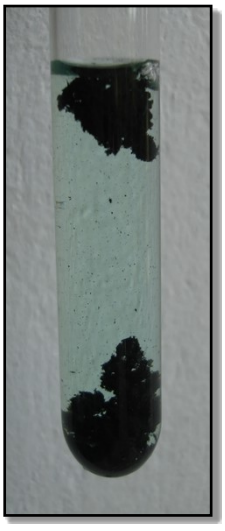

Fig. S1 GRR mediated oxidative dissolution of Ni nanowire when incubated in aqueous H_2SeO_3. Green colour of the solution indicates the presence of Ni^{2+} ions in solution.

DFT based structural analysis

Now a series of nickel selenide nanostructures with different crystalline phases have been reported from nickel and selenium. Owing to their close electronegativty (For Nickel = 1.91 and for selenium = 2.55), both stochiometric and non-stoichiometric phases are formed for example, $NiSe_2$, $Ni_{1-x}Se$ (x ranges from 0.85 to 1 w.r.t. 1 Se), Ni_3Se_2.[1] So for a critical understanding of the structures and the electronic properties of these NiSe based nanomaterials, we also performed DFT calculations on clusters of various NiSe structures. The initial symmetry for the input structures were obtained from the Inorganic Crystal Structure Database (ICSD). The initially retrieved structures of NiSe, $NiSe_2$, Ni_3Se_2 and Ni_3Se_4 were then relaxed using the conjugated gradient (CG) method, with force tolerance of 0.02 eV $Å^{-1}$. During the relaxation of the structure, no restrictions were imposed on the symmetry of the cell, volume of the cell or the position of atoms inside the cell. The energy cutoff for the plane waves was set to 500 eV. The k-mesh in the Brillouin zone was set as 3×3×3 and it was centered at the Γ-point. All the periodic calculations reported in this manuscript are obtained using the Vienna ab initio simulation package (VASP) code.[2] The projected augmented wave (PAW) method is chosen to represent the ionic potentials. The calculations were performed within the General-Gradient Approximation (GGA), and the Perdew-Burke-Ernzerhof (PBE) prescription for the exchange-correlation functional.[3,4] The computed lattice parameters are in very good agreement with the known crystal structures (within 2%) and the computed cohesive energies are -43.1 kJ/mol, -71.5 kJ/mol, -142.6 kJ/mol and -173.1 kJ/mol for NiSe, $NiSe_2$, Ni_3Se_2 and Ni_3Se_4 respectively. Clearly, the cohesive energy increases as the number of Ni and Se increase in the unit cell suggestive of strong bonding interactions. This is evident from the plots of electron localization functions (ELF) as shown in Fig. S2. The magnitude of ELF decreases in the series NiSe $\rightarrow$ $NiSe_2$ $\rightarrow$ Ni_3Se_2 $\rightarrow$ Ni_3Se_4 also indicating greater delocalization.

From the optimized structures of the unit cells, 4 × 4 × 4 supercells were constructed from where spherical clusters of diameter 1 nm were scooped out to derive the initial structures for the nanoparticles. The dangling atoms were removed and these structures were further optimized using the B3LYP version of DFT, which is comprised of Becke's hybrid, three-parameter, functional and the correlation functional of Lee, Yang, and Parr.[5,6] The LANL2DZ basis set was employed. Additional frequency calculations were performed to verify all real vibrational frequencies for the ground-state structures. The optimized structures for nanoparticles are shown in Fig. S3 Along with the structures, the density of

states (DOS) of the KS-orbitals are plotted. All these clusters show a small HOMO – LUMO gap of ~ 1 eV (0.83 eV, 1.18 eV, 0.61 eV and 0.74 eV for NiSe, $NiSe_2$, Ni_3Se_2 and Ni_3Se_4 respectively). The frontier KS-orbitals show significant delocalization of the electrons (HOMO and LUMO are shown in Fig. S4). Natural Bond Orbital (NBO) calculations[7] show that the average natural electron configurations for Ni and Se are $[Xe]4s^{0.32}3d^{9.13}4p^{0.51}$ and $[Xe]4s^{1.52}4p^{4.38}$ respectively suggesting strong hybridization between the atomic orbitals. The Ni–Se bonds in the clusters have almost equal contributions from both the Ni and Se atoms. This is also understood from the fact that for HOMO, the d-orbitals of Ni and the p-orbitals of Se contribute 33% and 17% respectively while for LUMO the contributions are 29% and 16% respectively.

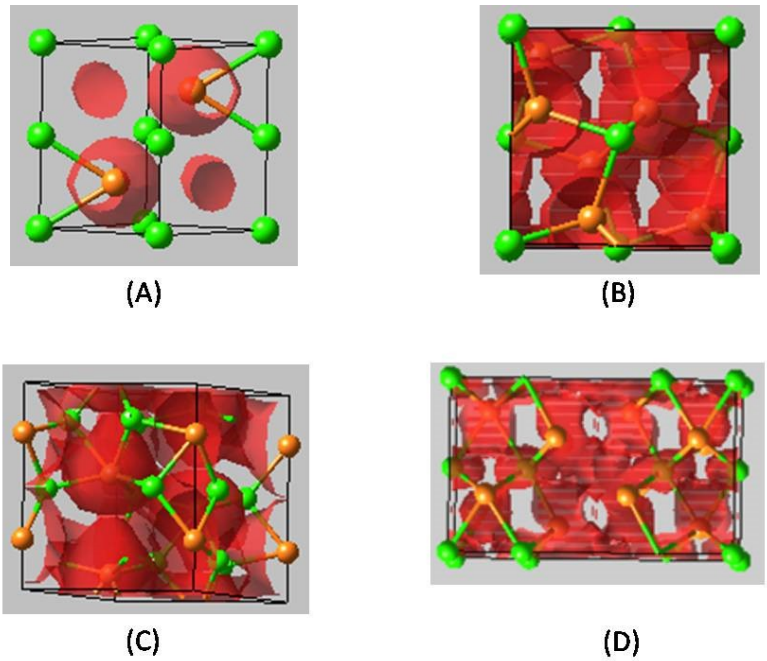

Fig. S2 Electron Localization Function (ELF) for (A) NiSe (isosurface value = 0.450), (B) $NiSe_2$ (isosurface value = 0.396), (C) Ni_3Se_2 (isosurface value = 0.249) and (D) Ni_3Se_4 (isosurface value = 0.177)

.

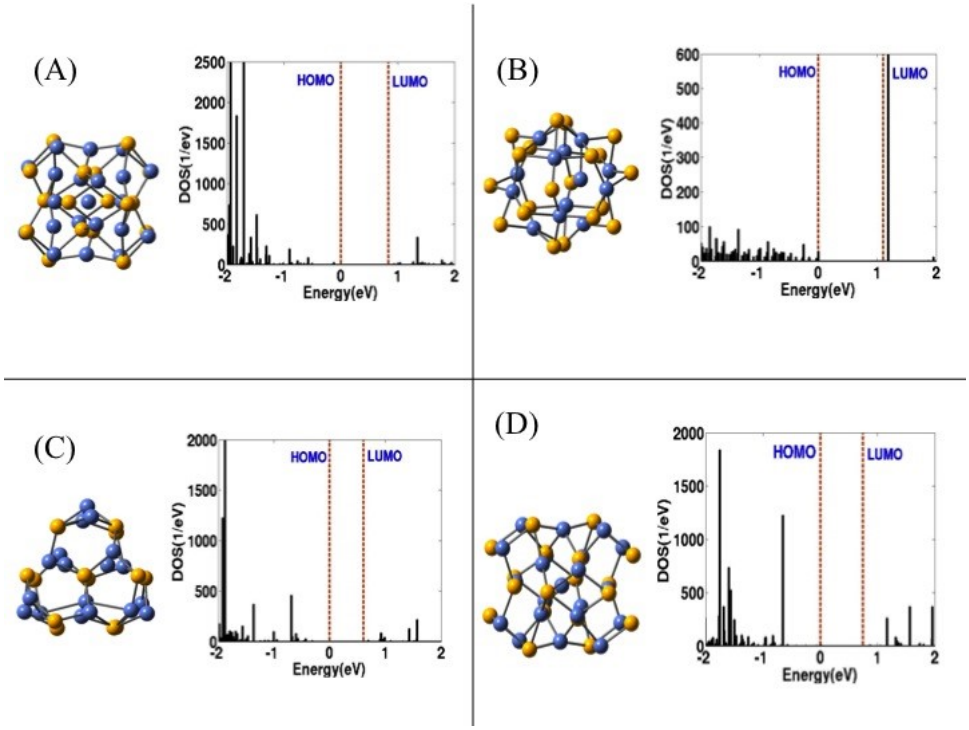

Fig. S3 Structures and density of states (DOS) for (A) NiSe, (B) $NiSe_2$, (C) Ni_3Se_2 and (D) Ni_3Se_4.

.

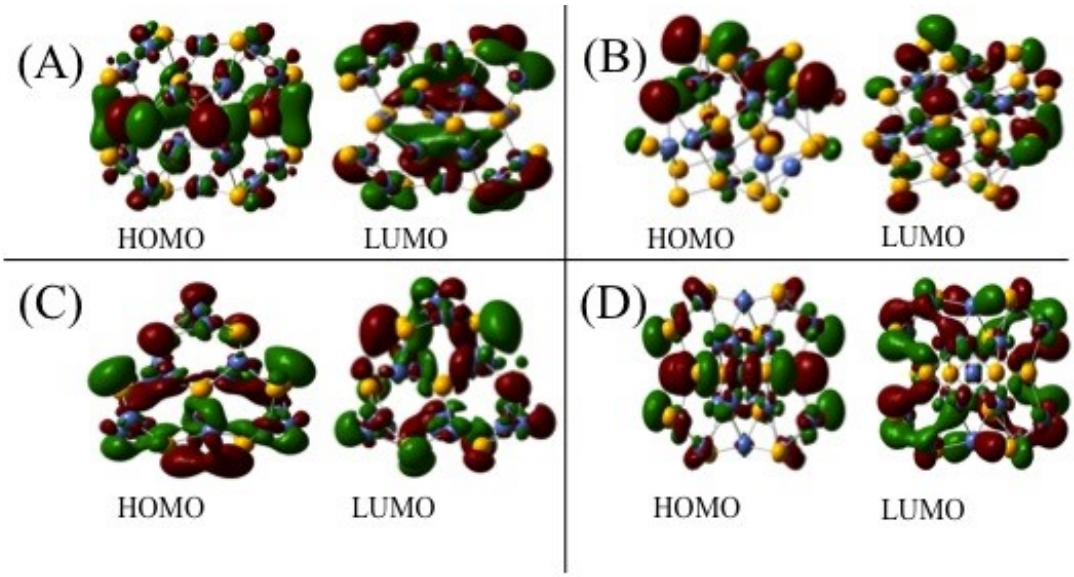

Fig. S4 Kohn-Sham frontier orbitals for (A) NiSe, (B) $NiSe_2$, (C) Ni_3Se_2 and (D) Ni_3Se_4.

References

1. Z. Zhuang, Q. Peng, J. Zhuang, X. Wang and Y. Li, *Chem. Eur. J.*, 2006, **12**, 211-217.

2. G. Kresse and J. Furthmüller, *Phys. Rev. B,*, 1996, **54**, 169-186.

3. J. P. Perdew, K. Burke and M. Ernzerhof, *Phys. Rev. Lett.*, 1996, **78**, 1396.

4. J. Heyd and G. E. Scuseria, *J. Chem. Phys.*, 2003, **118**, 8207-8215.

5. A. D. Becke, *J. Chem. Phys.*, 1993, **98**, 5648-5652.

6. C. Lee, W. Yang and R. G. Parr, *Phys. Rev. B,*, 1988, **37**, 169-186.

7. F. Weinhold and C. Landis, *Valency and Bonding, A Natural Bond Orbital Donor-Acceptor Perspective*, Cambridge University Press (2005).

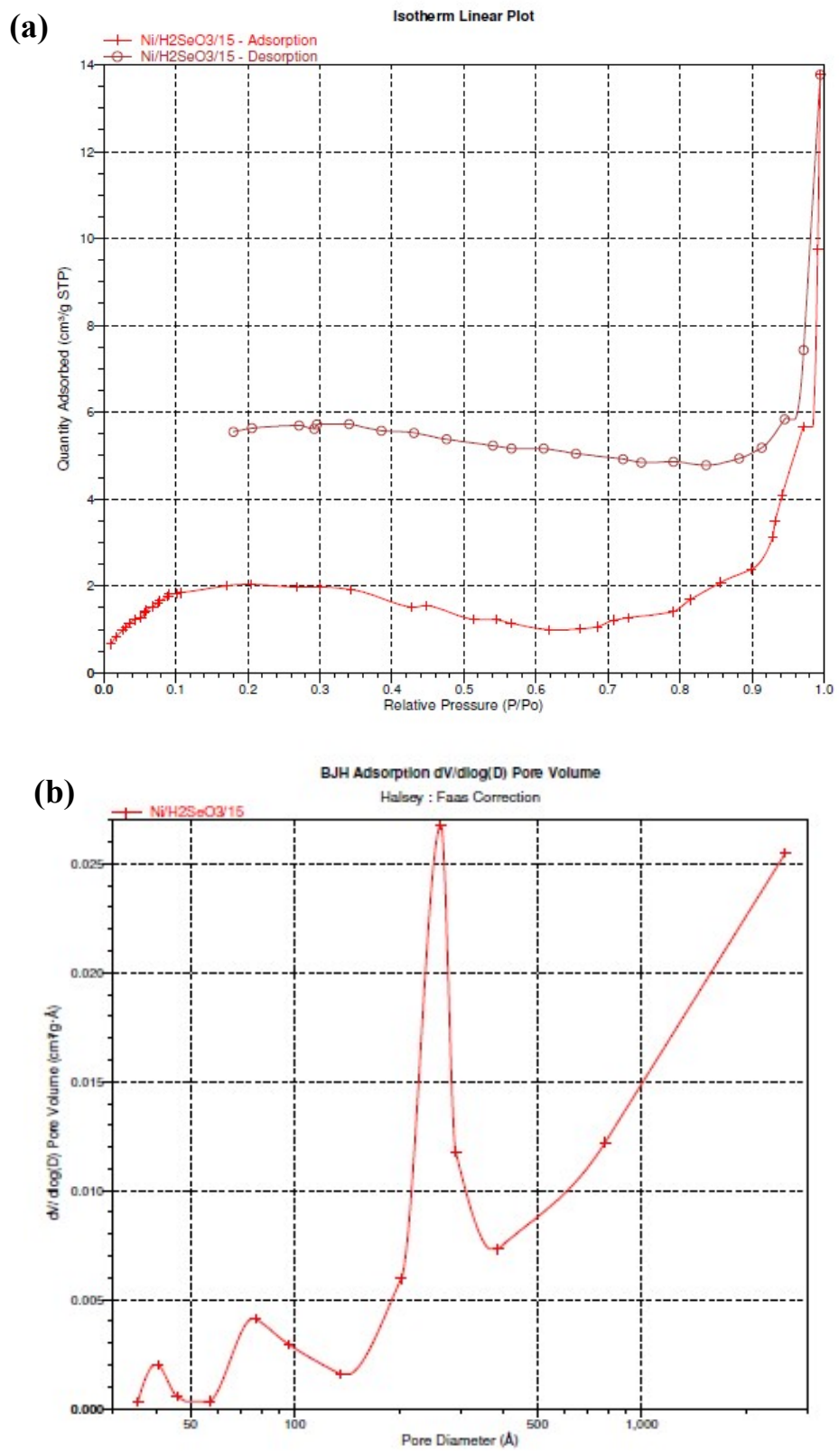

Fig. S5 (a) N_2 adsorption and desorption isotherm of the $NiSe_2$ nanotube. (b) Pore size distribution curve.

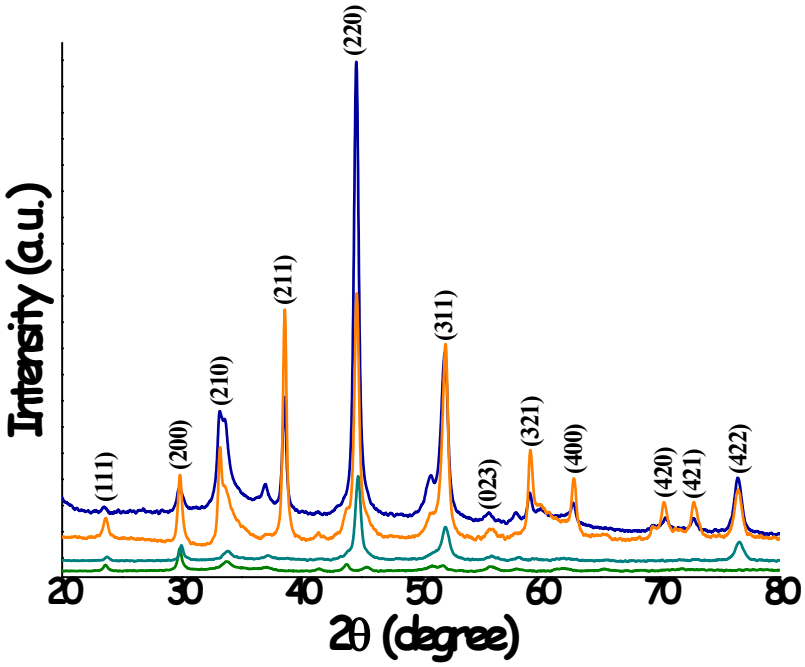

Fig. S6 Powder X-ray diffraction patterns of the as-synthesized $NiSe_2$ nanotubes synthesized at different time domains [5 days (green line), 10 days (sea-green line), 34 days (orange line) and 51 days (blue line) of continuous incubation at room temperature].

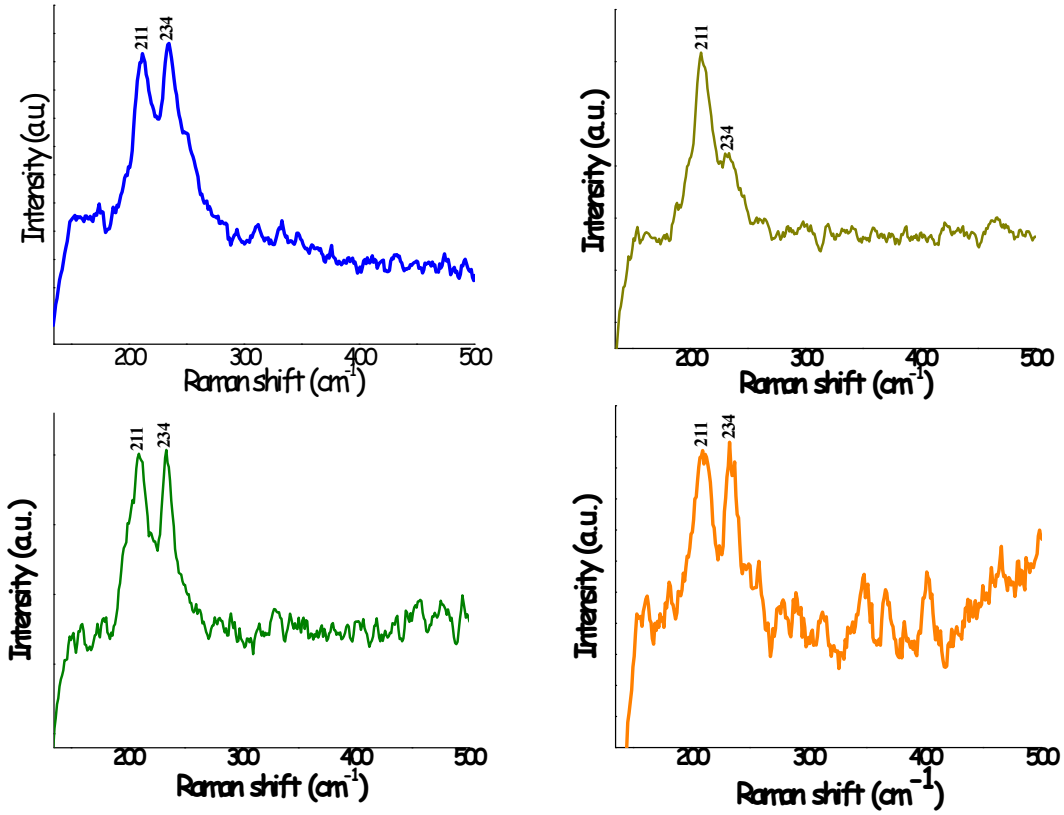

Fig. S7 Raman spectrum of the as-synthesized $NiSe_2$ nanotubes synthesized at different time domains [7 days (Blue), 25 days (Yellow), 45 days (Green) and 55 days (Orange) of continuous incubation at room temperature].

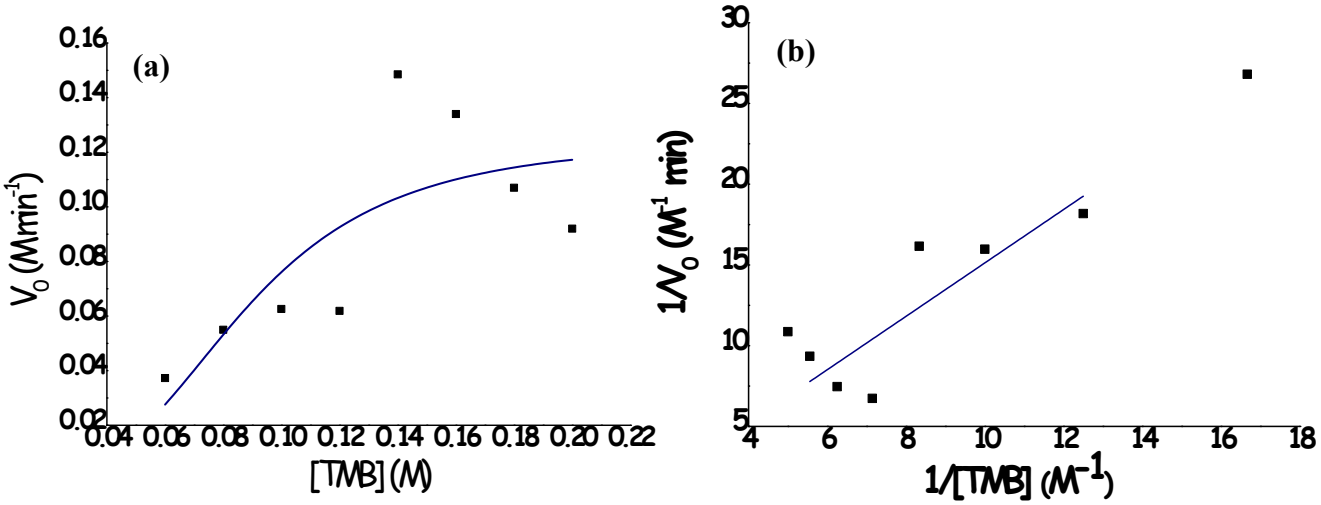

Fig. S8 (a) Plot of the initial rate of the reaction (V_0) vs substrate (TMB) concentration; (b) Lineweaver-Burk plot.

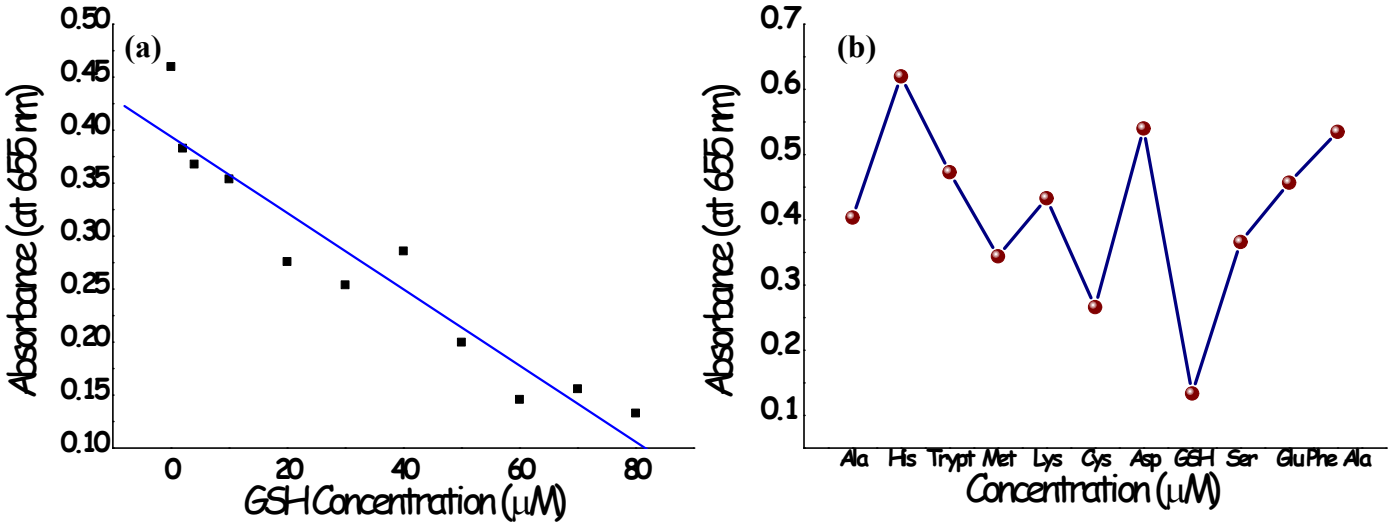

Fig. S9 (a) Plot of the Absorbance at 655 nm versus variable GSH concentration. (b) Plot of the Absorbance at 655 nm in presence of GSH and different amino acids other than GSH (Concentration: 80 μM). Reaction conditions remain same for all measurements.